Supplementary Text.

Two-step inactivation in Kv channels. Although inactivation of *Shaker* and Kv channels is commonly thought to reflect a single-step insertion of a hydrophobic N-terminal peptide into the narrow inner pore[1-3], a form of two-step inactivation has also been proposed in Kv channels[4,5] largely based on the idea that basic residues positioned downstream of the hydrophobic inactivation segment may influence inactivation kinetics through electrostatic interactions with the pore domain. Neutralization of N-terminal residues K18K19 in *Drosophila Sh*B[1,6] and R18 in *Aplysia* Kv1[5] markedly slow the development of inactivation. Whether such effects require postulation of additional steps in the Kv inactivation scheme probably requires further study and our results provide no additional insight on this question, but establish that steric interactions do not determine *Shaker* peptide binding affinity. If recovery of Shaker-IR channels from block by either L- or D-Shaker peptide involved a passage through a preinactivated open state (O*), our results (Fig 3) would suggest that occupancy of this state contributes little to net tail current flux and that recovery is still dominated by unblocking from the inactivated state, I. We prefer the view that any role of electrostatic interactions of Kv N-termini prior to interaction reflects positioning an N-terminus poised for subsequent activation during channel opening. Such a binding interaction would be unlikely to influence recovery from inactivation and would also not impact on the usual onset of inactivation, except to the extent that N-termini are not in the poised position. Irrespective of the mechanistic basis of electrostatic interactions in Kv interactions, this process seems quite distinct from the steric binding necessary for 2-step inactivation of the BK β3a N-terminus.

Figure S1. (a) BK β-subunit topology and sequence of the β3a N-terminus. BK β subunits contain two transmembrane segments. An extracellular loop (Out) contains four conserved cysteines in β1-β4 and four additional conserved cysteines in β2-β4 (orange balls: cysteines). The β subunits also contain cytosolic N-termini (N-term) and C-termini (C-term). The N-termini of β2, β3a, β3b, and β3c subunits mediate inactivation. The sequence of the 21 residue β3a-specific N-terminal insert is shown on the bottom.

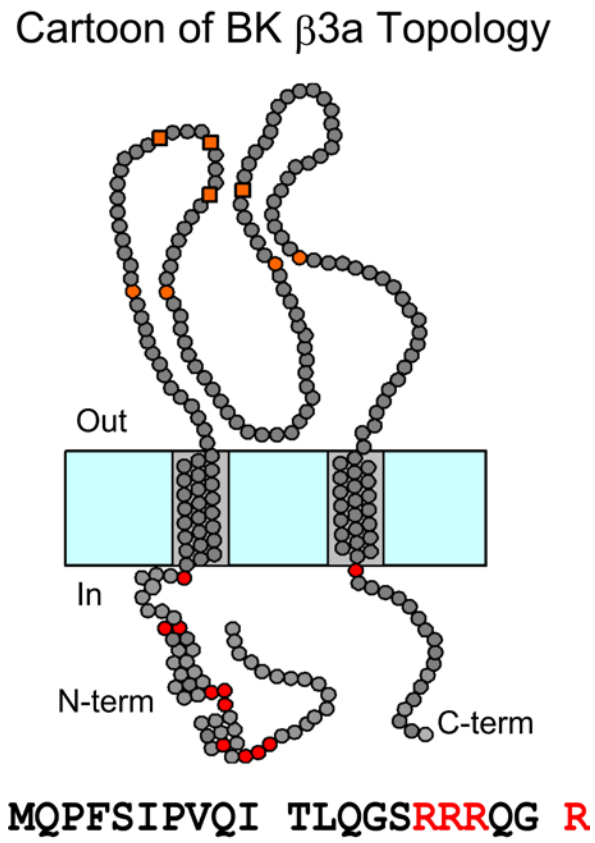

Figure S2. Characteristics of β3a-induced tails current openings are consistent with rapid oscillations between two states (O*-I*).

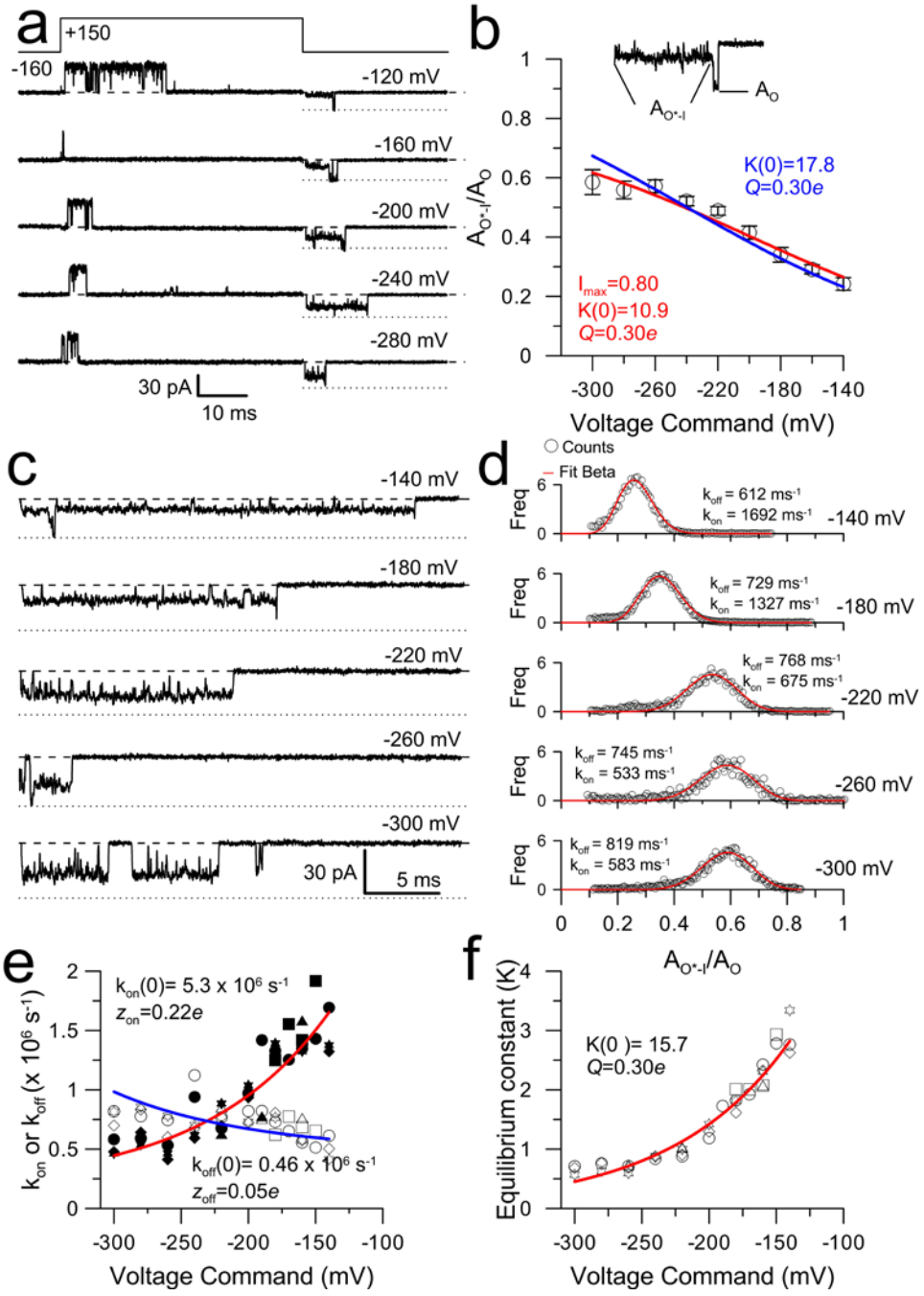

(a) The amplitude of the tail subconductance level relative to the full-open-amplitude varies with the voltage. Traces show a single BK channel obtained with 10 μM Ca^{2+} and 10 μM β3a(1-20) peptide in the intracellular solution, using the indicated voltage-protocol. Note that following repolarization the amplitude of the subconductance level relative to the full-open-amplitude (dotted lines) increases at more negative voltages. **(b)** Voltage dependence of the fractional amplitude of the tail subconductance level ($A_{O^*-I^*}/A_O$), calculated as the ratio between the averaged amplitude of the entire tail subconductance level and the corresponding

full-open-amplitude (see the inset) at each potential. Plot includes data from 5 patches containing 1 or 2 channels and points represent mean ± S.D. Solid lines correspond to fits of the following equation: $f(V) = f_{\max} / [1 + K(0) e^{\frac{-QFV}{RT}}]$, where $f(V)$ is the fractional amplitude of the tail subconductance level, $f_{\max}$ is the maximum value for the fractional amplitude, *K(0)* is the equilibrium constant (I/O*) at 0 mV, and Q describes the voltage dependence of the O*-I equilibrium. Based on the idea that the fractional amplitude reflects time-averaged occupancy of two states, O* and I, *f(V)* as given in the above equation explicitly reflects O*/(O*+I). With k_{on} and k_{off} as the forward (O*→I) and reverse (I→O*) transitions, respectively, the fractional amplitude can also be expressed as $f(V)=k_{off}(V)/(k_{off}(V)+k_{on}(V))$. The two fitted lines assume that the overall voltage-dependence of K(V) is 0.3*e* as defined in panel **(f)** below. Furthermore, we make two assumptions regarding f_{max}. For the blue line, f_{max} was constrained to 1.0, which assumes that only the O*-I* equilibrium defines the fractional amplitude. For the red line, the best fit yielded f_{max}= 0.80 ± 0.7, which would require that some other process other than K(V) must also contribute to the fractional amplitude estimate. For the blue line, *K(0)*=17.8 ±1.6, and, for the red, *K(0)*=10.9 ± 3.1. Overall, kinetic and equilibrium estimates for properties of the O*/I* equilibrium based on an independent method used in **(d-f)** account very well for the average fractional amplitude of the subconductance level. **(c)** Subconductance and full openings following repolarization from the same patch as in **(a)** are shown on a faster time base. **(d)** The characteristics of the tail subconductance level are consistent with rapid unresolved transitions between 2 states (O*-I*). Amplitude histograms at each potential were compiled from the corresponding tail current trace shown at left **(c)** together with another 4-7 tail traces recorded at the same conditions in the same patch. Amplitude histograms are plotted as frequency of occurrence vs. fractional amplitude (relative to full-open-amplitude). We calculated the theoretical amplitude distributions applying a Beta-function, which assumes that the amplitude is composed of filtered fluctuation between 2 discrete conductance states [7]. Theoretical amplitude distribution only depends on the transition rates between the two states and the filter cutoff frequency, according to the equation:

$$B(a,b) = A^{a-1}(1-A)^{b-1}; a = k_{off} * \tau, b = k_{on} * \tau$$

where A is the fractional amplitude, k_{on} and k_{off} are the forward (O*→I*) and reverse (I*→O*) transitions, respectively, and τ is the filter time constant. Using the filter cutoff frequency of the real data acquisition (0.0228), the rates (k_{on} and k_{off}) were adjusted to give the best fit of the theoretical amplitude distribution to the measured amplitude histogram at each potential (solid red line). The excellent fits between the predicted and the measured amplitude histogram strongly support the assumption. Values of k_{on} and k_{off} obtained from each fit are shown above each plot and support the view that oscillations between O*-I* states are exceedingly rapid. **(e)** Voltage dependence of transition rates obtained in 5 different patches following the same procedure as in **(d)**. k_{on} (open symbols), k_{off} (filled symbols). Values for k_{on} were fitted to an exponential: $k_{on}(V) = k_{on}(0) e^{\frac{-z_{on}FV}{RT}}$ (solid line), where $k_{on}(0)$ is the transition rate at 0 mV, z reflects voltage-dependence of the rate, and other parameters are as in (a), with $k_{on}(0)$=5.3(±1.0)*10^6 s^{-1} with z_{on} = 0.22*e* ± 0.3*e*. For $k_{off}(V)$, $k_{off}(0)$=0.46(±0.07)*10^6 s^{-1} with z_{off} = 0.05*e* ± 0.02*e*. **(f)** Voltage dependence of the equilibrium constant (k_{on}/k_{off}) calculated from the corresponding rates in **(e)**. Solid line represents the fit to the exponential $K(V) = K(0) e^{\frac{-QFV}{RT}}$ with *K(0)*=15.7 ± 2.1 and Q = 0.30*e* ± 0.02*e*, with *K(0)* the equilibrium constant at 0 mV. The origins of the voltage-dependence in these transitions rates remain unknown[8].

Figure S3. β3a(1-21) L-peptide exhibits no intrinsic structure.

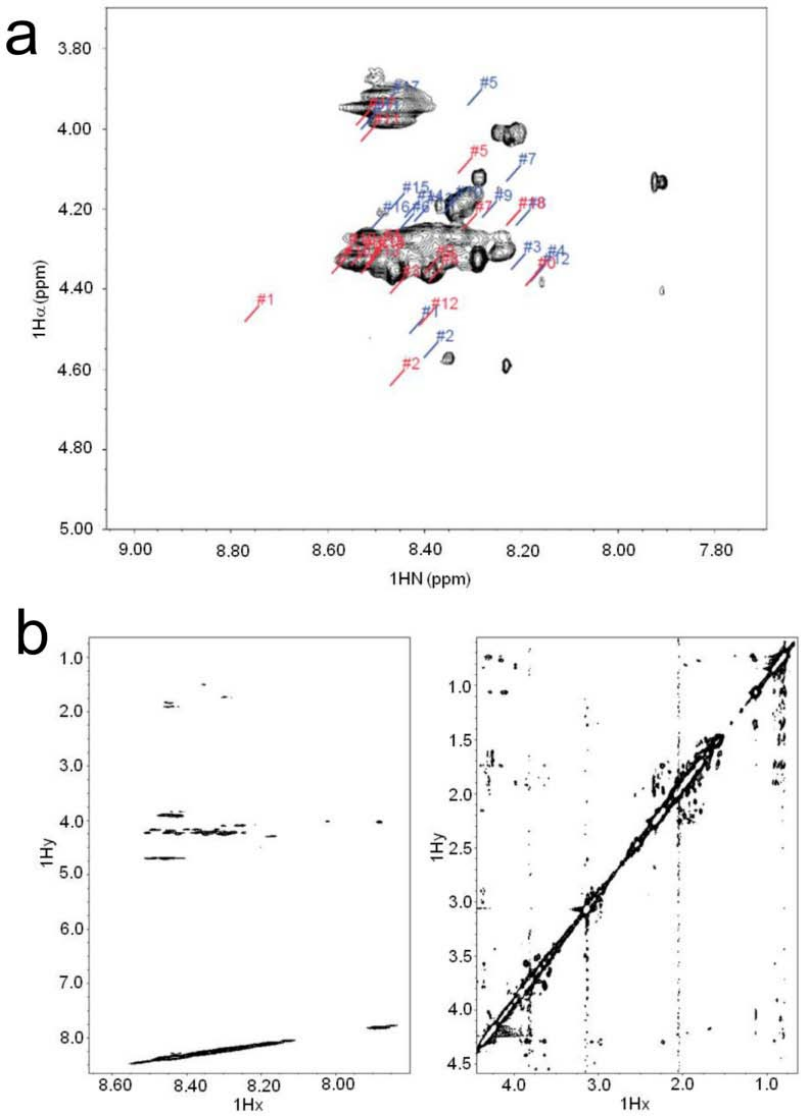

(a) TOCSY spectrum of β3a(1-21) L-peptide reveals very little dispersion in the H_α and H_N chemical shifts, typical of an unstructured peptide. Neighbor-corrected random coil chemical shifts were calculated for the β3a(1-21) peptide sequence using the ncIDP web interface at www.protein-nmr.org[9] and the random coil chemical shifts of Tamioloa (blue[9]) and Schwarzinger (red[10]). The chemical shifts predicted for a random coil structure based only on the amino acid sequence vary slightly depending on the reference tables used. However, the observed chemical shift values and dispersion agree quite closely with the calculated shifts, supporting a random coil structure for this peptide. β3a(1-21) D-peptide is very similar indicating a lack of intrinsic structure in that peptide as well. **(b)** ^1H-^1H NOESY spectra of the β3a(1-21) L-peptide reveal minimal crosspeaks in either the amide region (left) or aliphatic region (right). Comparison with ^1H-^1H TOCSY spectra of the L-peptide confirms that almost all NOEs are intra-residue, consistent with intrinsic disorder. Spectra of the D-peptide are indistinguishable.

Figure S4. β3a(1-21) L-peptide blocks with stronger apparent affinity than the β3a(1-21) D-peptide.

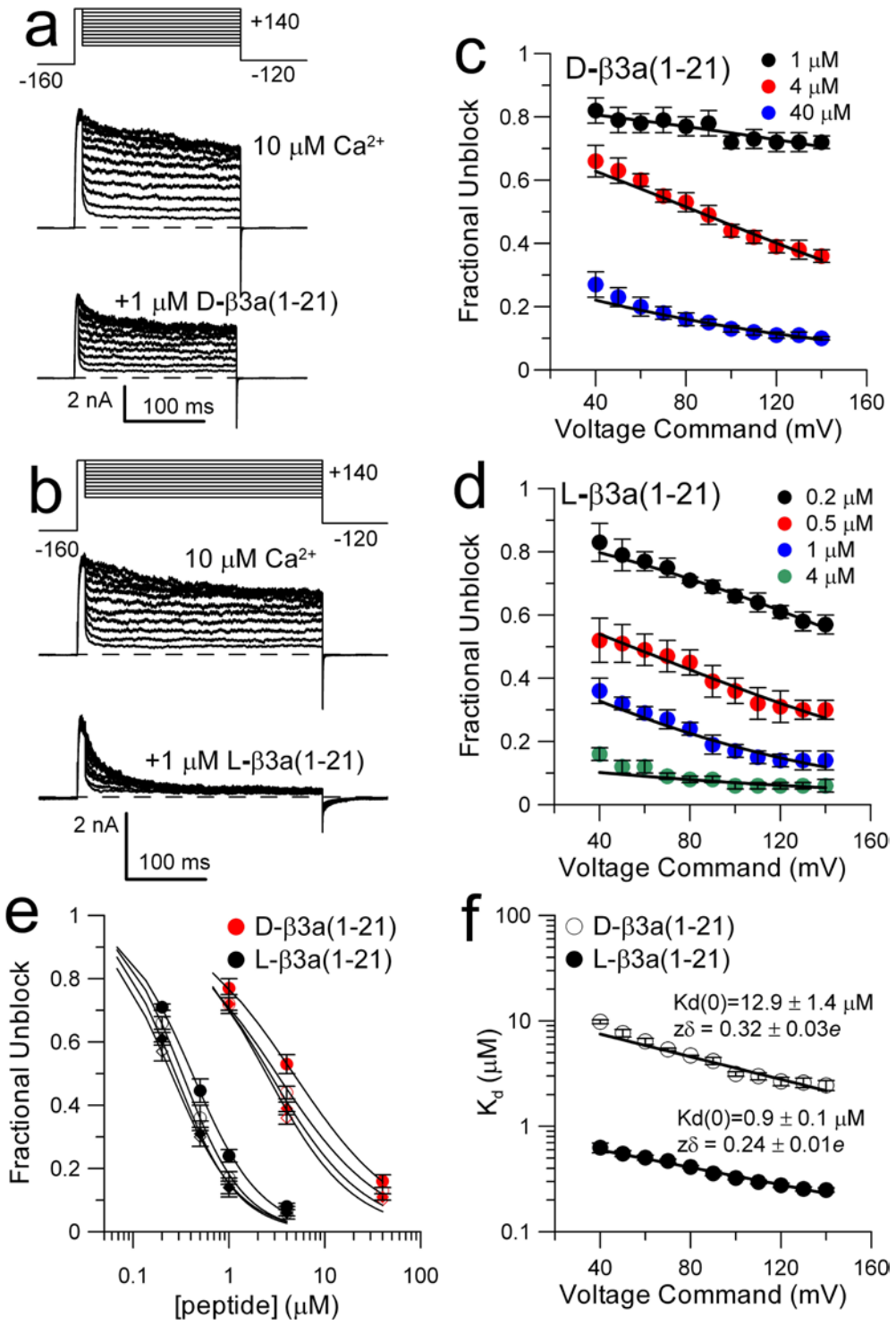

(a), (b) Currents evoked by the indicated protocol (10 μM cytosolic Ca^{2+}) in the absence (upper) and presence (bottom) of 1 μM of D-β3a **(a)** or L-β3a **(b)** peptide, respectively. Channels were maximally activated by a short pulse to +140 and then returned to potentials from +140 to +40 mV, to allow steady-state block in the presence of peptides. Each trace is an

average of 5 sweeps. Both peptides were tested with at least 3 different concentrations. **(c), (d)** Voltage dependence of block at different peptide concentrations for D-β3a **(c)** and L-β3a **(d)** peptides, respectively. Fractional unblock was calculated from the ratio between remaining current in the presence of peptide and the control current at steady state ($I_{peptide}/ I_{control}$). Points are means ± SEM from 4-6 different patches. Solid lines represents the independent fit to each concentration to a Woodhull equation [11] of the form: $I_{peptide}/ I_{control} = 1/(1+[peptide]/K_d(0)*e^{-z\delta FV/RT})$), where $K_d(0)$ is the apparent block equilibrium constant at 0 mV and zδ describes the voltage dependence of block. Values of $K_d(0)$ and zδ obtained from the fits are: for 1 μM D-β3a, $K_d(0)$=5.2 μM and zδ=0.14*e*; for 4 μM D-β3a, $K_d(0)$=10.7 μM and zδ = 0.29*e*; for 40 μM D-β3a, $K_d(0)$=16.7 μM and zδ=0.25*e*; for 0.25 μM L-β3a, $K_d(0)$=1.2 μM and zδ=0.29*e*; for 0.5 μM L-β3a, $K_d(0)$=0.9 μM and zδ=0.29*e*; for 1 μM L-β3a, $K_d(0)$=8 μM and zδ=0.32*e*; for 4 μM L-β3a, $K_d(0)$=0.6 μM and zδ=0.18*e*. **(e)** Fractional unblock current was plotted against [peptide] at potentials from +140 (open diamonds), +120 (filled diamonds), +100 (open circles), and +80 (filled circles) mV and points were fit to the Hill equation: $I_{peptide}/ I_{control}=1/(1+([peptide]/K_d)^n)$, where K_d is the apparent equilibrium constant and n is the Hill coefficient. Values of K_d and n obtained from the fits are: for D-β3a, K_d=4.7 μM and n=0.77 at +80 mV, K_d=3.1 μM and n=0.78 at +100 mV, K_d=2.7 μM and n=0.88 for +120 mV and K_d=2.4 and n=0.96 for +140 mV; for L-β3a peptide, K_d=0.4 μM and n=1.21 for +80 mV), K_d=0.32 μM and n=1.34 at +100 mV, K_d=0.27 μM and n=1.33 at +120 mV and K_d=0.25 μM and n=1.22 for +140 mV. **(f)** K_ds from the Hill equation fits in **(e)** were plotted as a function of voltage. Error bars represent the s.d of the Hill fits in **(e)**. Solid lines represent the fits to: $K_d(V)=K_d(0)* e^{-z\delta FV/RT}$. The apparent $K_d(0)$ differs by more than 10-fold between the D and L-peptides with each having similar voltage-dependence.

Figure S5. Neutralization of residues R16, R17, and R18 on the full mβ3a subunit does not disrupt two-step inactivation.

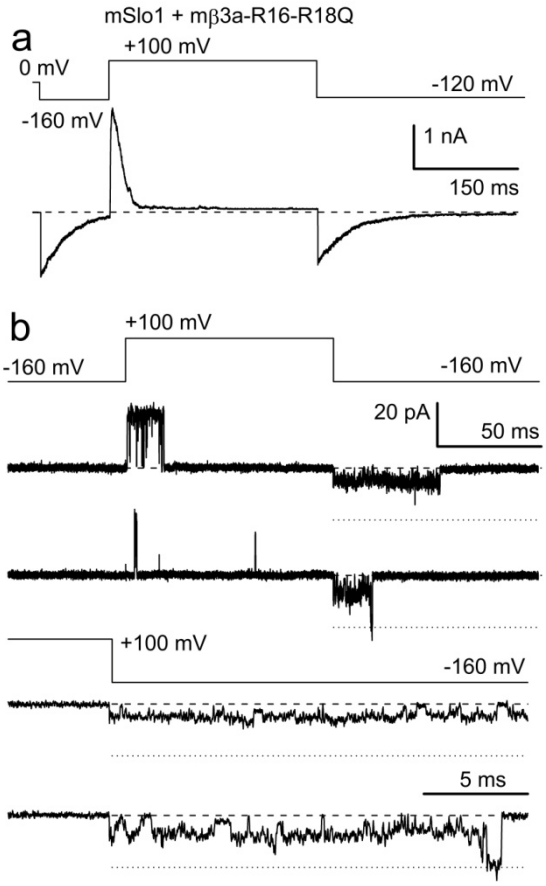

(a) Currents arising from channels formed from *mSlo1* α and mβ3a-R16Q/R17Q/R18Q were activated with the indicated voltage-protocol with 10 μM Ca^{2+} in an inside-out patch. Inactivation generally similar to that from wt β3a is observed along with the characteristic slow tail current following repolarization. **(b)** An inside-out patch containing two active α+β3a-R16Q/R17Q/R18Q channels was stimulated with the indicated voltage-protocol with 10 μM cysotolic Ca^{2+}. The selected traces show openings from only one of the two channels in the patch. Repolarization is associated with instantaneous low current amplitude, high variance openings often terminating in a full opening. The bottom two traces show the tail openings on a faster time base to highlight the instantaneous nature of the low current level openings following repolarization. These features are consistent with the two-step inactivation behavior observed for wt β3a N-termini. Since the β3a(1-20) peptide is sufficient to produce the characteristic two-step inactivation behavior and all the basic residues in the first 20 residues of the intact β3a N-terminus can be neutralized without disrupting two-step inactivation, this indicates that electrostatic interactions do not participate in the steric binding interaction essential to produce β3a-mediated two-step inactivation.

Figure S6. *Shaker*-like non-specific unblocking events do occur at low frequency with β3a L-peptide. We hypothesize that the β3a L-peptide should occasionally produce unblocking events similar to those observed with the D-peptide (Fig. 2). Since the β3a peptide blocks with about 13-fold higher affinity than the D-peptide (Fig. S4), if the L-peptide can also bind in a fashion similar to the D-peptide, one might expect that at the end of an inactivating voltage step D-peptide-type unblock events might be observed at something less than 10% of the time.

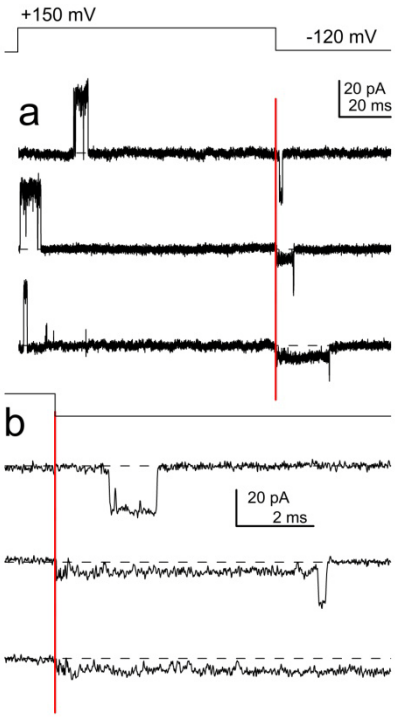

(a) Traces show a single BK channel activated with the indicated (top) voltage protocol with 10 μM Ca^{2+} and bathed with 10 μM L-β3a peptide(1-20). For the top trace, following repolarization (red line) a full channel opening is observed, while for the other top traces the characteristic β3a reduced current events are seen. **(b)** The traces from (**a**) are shown on an expanded time scale, showing the almost 2 ms delay before the opening for the top trace, with no indication of any delay for the two lower traces. We examined a total of 894 traces from 5 patches in which single BK channels were activated with a 100 ms depolarizing step to +150 mV in the presence of 10 μM β3a L-peptide. For this set of traces, 697 showed small conductance openings (77.96%) with no latency, while 22 (2.46%) exhibited a finite delay after repolarization. These results support the idea that the following scheme more fully describes blockade by free β3a L-peptide.

$$C \rightleftharpoons O \rightleftharpoons O^* \rightleftharpoons I^*$$
$$\uparrow\downarrow$$
$$I$$

Figure S7. L- and D- *Shaker* Ball peptides block *Shaker*-IR channels with similar affinities and kinetics.

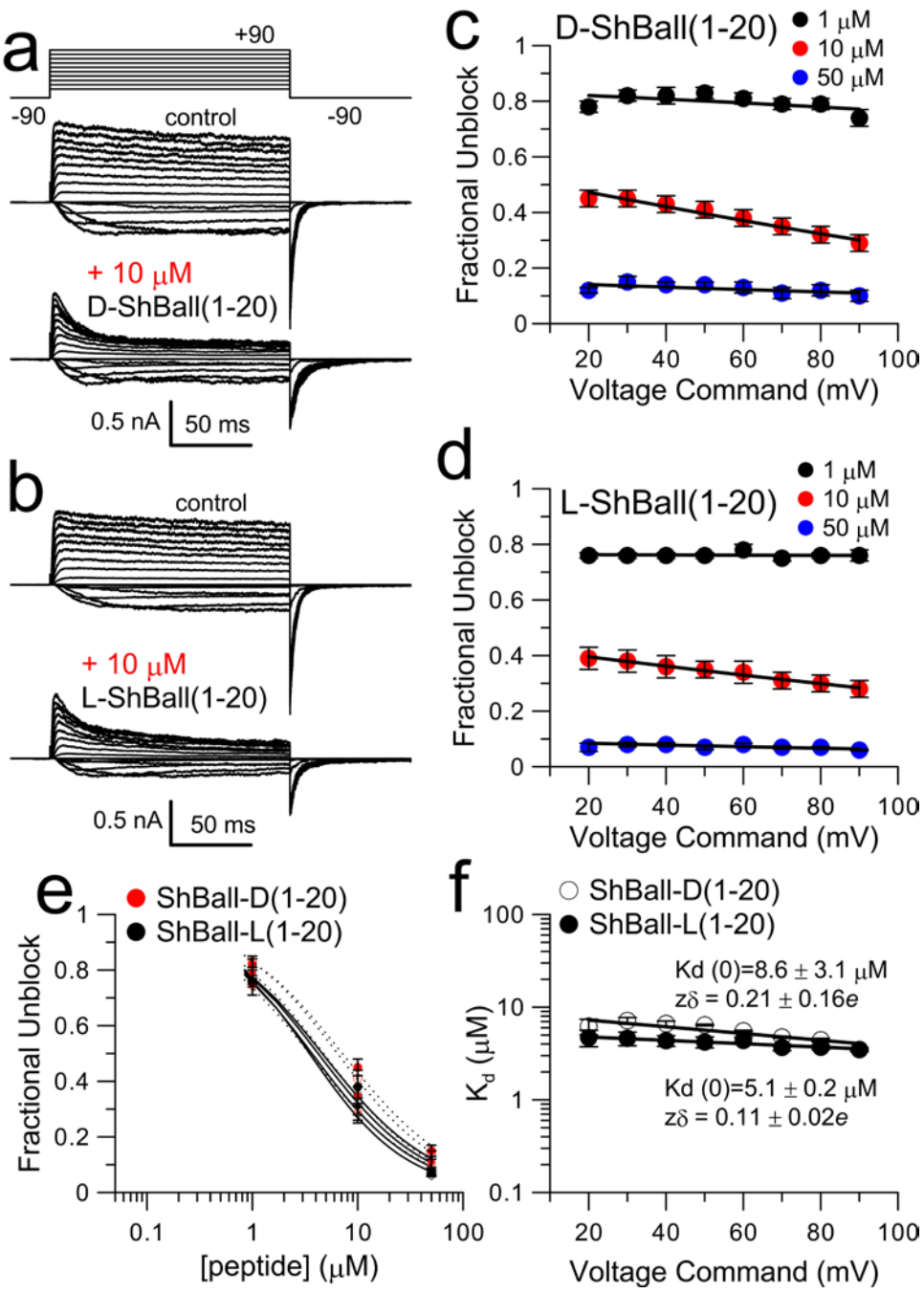

(a), (b) Currents evoked by the indicated protocol in the absence (upper) and presence (bottom) of 10 μM of D-Shaker(1-20) **(a)** or L-Shaker(1-20) **(b)** peptide, respectively. Channels were activated by steps from -70 to +90 following a prepulse to -90 mV. **(c), (d)** Voltage dependence of block at different peptide concentrations for (c) D-Shaker(1-20) peptide and (d) L-Shaker(1-20) peptide, respectively. Fractional unblock was calculated from the ratio between remaining current in the presence of peptide and the control current at steady state ($I_{peptide}/I_{control}$). Points are means ± SEM from 4-5 different patches. Solid lines represents the independent fit of each concentration data set to a Woodhull equation[11] of the form: $I_{peptide}/$

$I_{control}$ =1/(1+[peptide]/K_d(0)*$e^{-z\delta FV/RT}$)), where K_d(0) is the apparent block equilibrium constant at 0 mV and zδ describes the voltage dependence of block. Values of K_d(0) and zδ obtained from the fits are: for 1 μM D-Sh(1-20), K_d(0)=5.0 μM and zδ=0.11*e*; for 10 μM D-Sh(1-20), K_d(0)=11.1 μM and zδ = 0.27*e*; for 50 μM D-Sh(1-20), K_d(0)=8.9 μM and zδ=0.10*e*; for 1 μM L-Sh(1-20), K_d(0)=3.2 μM and zδ=0.01*e*; for 10 μM L-Sh(1-20), K_d(0)=7.5 μM and zδ=0.2*e*; for 50 μM L-Sh(1-20), K_d(0)=5.1 μM and zδ=0.11*e*; **(e)** Fractional unblock was plotted against [peptide] at potentials of +90 (open diamonds), +70 (filled diamonds), +50 (open circles), and +30 (filled circles) mV and points were fit to the Hill equation: $I_{peptide}$/ $I_{control}$=1/(1+([peptide]/K_d)^n), where K_d is the apparent equilibrium constant and n is the Hill coefficient. Values of K_d and n obtained from the fits are: for D-Sh(1-20), K_d=3.5 μM and n=0.83 at +90 mV, K_d=4.8 μM and n=0.86 at +70 mV, K_d=6.4 μM and n=0.86 for +50 mV and K_d=7.1 and n=0.92 for +30 mV; for L-Sh(1-20) peptide, K_d=3.5 μM and n=0.94 for +90 mV, K_d=3.7 μM and n=0.87 at +70 mV, K_d=4.2 μM and n=0.86 at +50 mV and K_d=4.6 μM and n=0.88 for +30 mV. **(f)** K_ds from the Hill equation fits in **(e)** were plotted as a function of voltage. Error bars represent the s.d of the Hill fits in **(e)**. Solid lines represent the fits to: $K_d(V)=K_d(0)* e^{-z\delta FV/RT}$. The apparent K_d(0) differs by less than 2-fold between the D and L-peptides with values for K_d(0) and zδ given on the figure.

Figure S8. The ability of cytoplasmic pore blockers to influence inactivation onset and recovery can provide insight into details of inactivation mechanism.

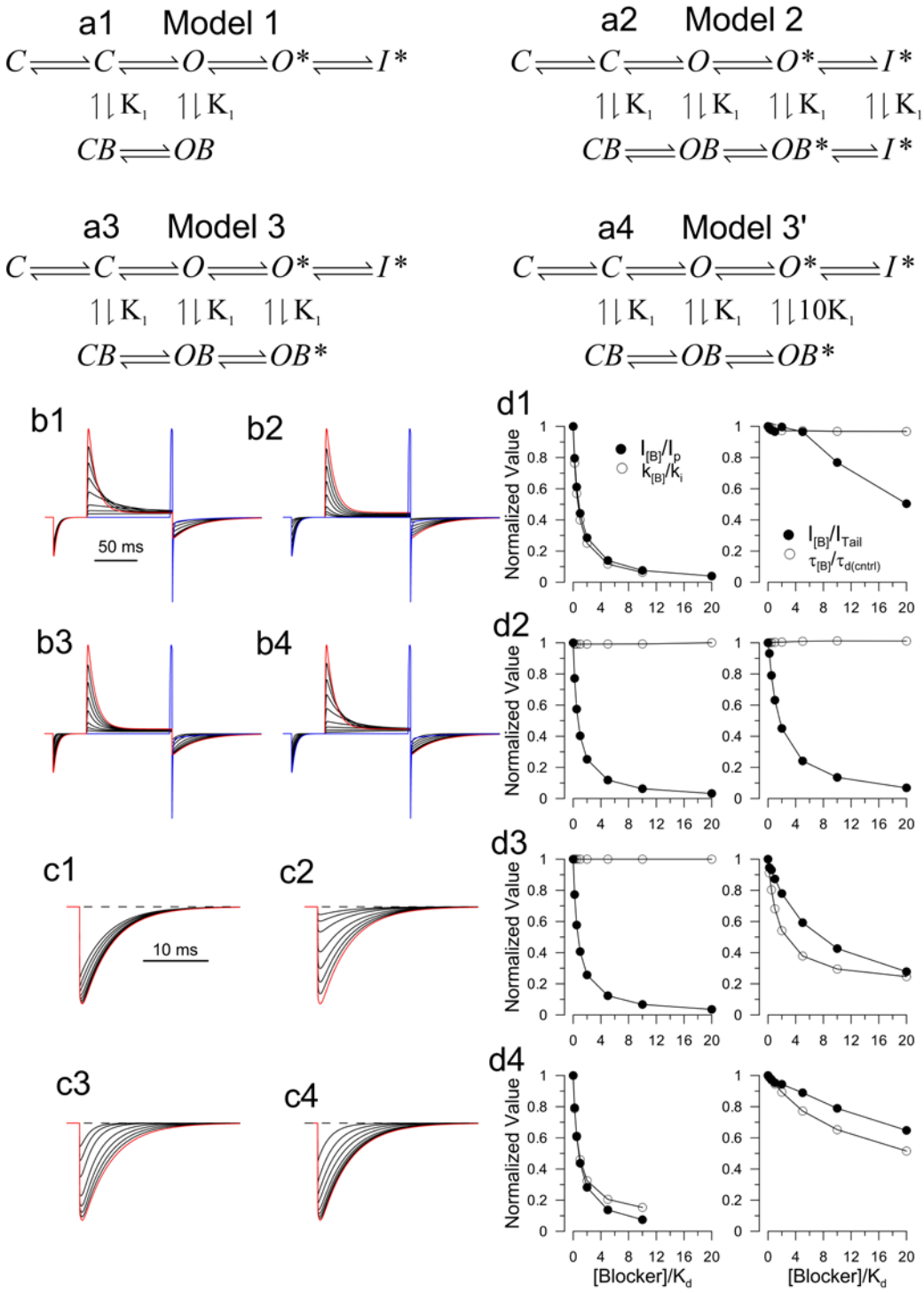

(a) Two-step inactivation models in the presence of pore-blocker. **a1,** Model 1: blocker binds to open and closed channels, but when the β3a N-terminus moves into the pore, blocker can no longer bind to the O* state. **a2**, Model 2: blocker can bind to any of the states in the activation-inactivation gating scheme. **a3**, Model 3: blocker binds within the central cavity and blocker binding prevents movement of the bound N-terminus into its inactivating position. **a4**, Model

3', blocker acts as in panel **a3**, but blocker affinity within the pore is reduced by the presence of the N-terminus in the preinactivated position. **(b1-b4)** Currents were simulated from the Models in **a1-a4**. Rates of transitions among states in the primary activation/inactivation pathway were: k_{12}=500exp(0.5V/kT); k_{21}=100exp(-0.5V/kT); k_{23}=250exp(0.5V/kT); k_{32}=200exp(-0.5V/kT); k_{34}=50exp(0.2V/kT); k_{43}=4exp(-1V/kT); k_{45}=100000exp(0.1V/kT); k_{54}=10000exp(-0.1V/kT). Rates of recovery from block were 10000 s^{-1} (z = 0.05*e*) in all cases, and the forward rate varied between 2000 s^{-1} and 200000 s^{-1} (z=0.05*e*), spanning a range of 0.2 to 50 times the effective K_d of block. Block/unblock rates were chosen to reflect experimental observations and channel activation rates chosen to approximate BK activate and deactivation rates. For model a4, to maintain microscopic reversibility, the forward rate of block in the O*→ O*B transition was slowed 10-fold while the OB→OB* transition was slowed by a similar factor. **(b1)** Only the initial open state (O) can be blocked. This results in a slowing in inactivation onset similar to a simple-open channel block situation. No effect on the deactivation time course is observed. **(b2)** Both open states and the inactivation state can all be blocked identically. This results in no change in inactivation onset or deactivation time course. **(b3)** Both open states can be blocked, but block is competitive with entry into I. This results in no effect on inactivation onset, since block does not impede the rate limiting transition O→O* in the onset of inactivation. Competition between blocker and inactivation predicts an acceleration of the tail current time course. **(b4)** The affinity of block for O* is weakened 10-fold. This results in some slowing of the inactivation onset, while also predicts an increase in deactivation rates. (**c1-c4**) The tail currents from **b1-b4** are shown on a faster time base. **(d1-d4)** Peak outward current and inactivation time constant measured from simulated currents **(b1-b4)** as a function of [Blocker] are shown on the left, while peak tail current and deactivation time constant (from **c1-c4**) are plotted on the right.

Supplementary References

1 **Hoshi, T., Zagotta, W. N. & Aldrich, R. W. Biophysical and molecular mechanisms of Shaker potassium channel inactivation. *Science* 250, 533-538 (1990).**

2 **Demo, S. D. & Yellen, G. The inactivation gate of the Shaker K^+ channel behaves like an open- channel blocker. *Neuron* 7, 743-753 (1991).**

3 **Gonzalez, C., Lopez-Rodriguez, A., Srikumar, D., Rosenthal, J. J. & Holmgren, M. Editing of human K(V)1.1 channel mRNAs disrupts binding of the N-terminus tip at the intracellular cavity. *Nat Commun* 2, 436, doi:ncomms1446 [pii] 10.1038/ncomms1446 (2011).**

4 **Zhou, M., Morais-Cabral, J. H., Mann, S. & MacKinnon, R. Potassium channel receptor site for the inactivation gate and quaternary amine inhibitors. *Nature* 411, 657-661 (2001).**

5 **Prince-Carter, A. & Pfaffinger, P. J. Multiple intermediate states precede pore block during N-type inactivation of a voltage-gated potassium channel. *J. Gen. Physiol.* 134, 15-34 (2009).**

6 **Murrell-Lagnado, R. D. & Aldrich, R. W. Interactions of amino terminal domains of Shaker K channels with a pore blocking site studied with synthetic peptides. *J. Gen. Physiol.* 102, 949-975 (1993).**

7 **Yellen, G. Ionic permeation and blockade in Ca^{2+}-activated K^+ channels of bovine chromaffin cells. *J. Gen. Physiol.* 84, 157-186 (1984).**

8 **Lingle, C. J., Zeng, X.-H., Ding, J.-P. & Xia, X.-M. Inactivation of BK channels mediated by the N-terminus of the β3b auxiliary subunit involves a**

two-step mechanism: possible separation of binding and blockade. *J. Gen. Physiol.* 117, 583-605 (2001).

9 **Tamiola, K., Acar, B. & Mulder, F. A. Sequence-specific random coil chemical shifts of intrinsically disordered proteins. *J Am Chem Soc* 132, 18000-18003 (2010).**

10 **Schwarzinger, S. *et al.* Sequence-dependent correction of random coil NMR chemical shifts. *J Am Chem Soc* 123, 2970-2978 (2001).**

11 **Woodhull, A. Ionic Blockade of Sodium Channels in Nerve. *J. Gen. Physiol.* 61, 687-708 (1973).**